Environmental Toxicology and Chemistry—Volume 39, Number 2—pp. 323–334, 2020
Received: 7 July 2019 | Revised: 25 October 2019 | Accepted: 30 October 2019

Environmental Chemistry

Development of a Novel Equilibrium Passive Sampling Device for Methylmercury in Sediment and Soil Porewaters

James P. Sanders,[a] Alyssa McBurney,[b] Cynthia C. Gilmour,[b] Grace E. Schwartz,[b] Spencer Washburn,[b] Susan B. Kane Driscoll,[c] Steven S. Brown,[d] and Upal Ghosh[a,*]

[a]Department of Chemical, Biochemical, and Environmental Engineering, University of Maryland Baltimore County, Baltimore, Maryland, USA
[b]Smithsonian Environmental Research Center, Edgewater, Maryland, USA
[c]Exponent, Maynard, Massachusetts, USA
[d]The Dow Chemical Company, Midland, Michigan, USA

Abstract: We explored the concept of equilibrium passive sampling for methylmercury (MeHg) using the strategy developed for hydrophobic organic chemicals. Passive sampling should allow prediction of the concentration of the chemically labile fraction of MeHg in sediment porewaters based on equilibrium partitioning into the sampler, without modeling diffusion rates through the sampler material. Our goals were to identify sampler materials with the potential to mimic MeHg partitioning into animals and sediments and provide reversible sorption in a time frame appropriate for in situ samplers. Candidate materials tested included a range of polymers embedded with suitable sorbents for MeHg. The most promising were activated carbon (AC) embedded in agarose, thiol–self-assembled monolayers on mesoporous supports embedded in agarose, and cysteine-functionalized polyethylene terephthalate, which yielded log sampler–water partition coefficients of 2.8 to 5 for MeHgOH and MeHg complexed with dissolved organic matter (Suwannee River humic acid). Sampler equilibration time in sediments was approximately 1 to 2 wk. Investigation of the MeHg accumulation mechanism by AC embedded in agarose suggested that sampling was kinetically influenced by MeHg interactions with AC particles and not limited by diffusion through the gel for this material. Also, AC exhibited relatively rapid desorption of Hg and MeHg, indicating that this sorbent is capable of reversible, equilibrium measurements. In sediment:water microcosms, porewater concentrations made with isotherm-calibrated passive samplers agreed within a factor of 2 (unamended sediment) or 4 (AC-amended sediment) with directly measured concentrations. The present study demonstrates a potential new approach to passive sampling of MeHg. *Environ Toxicol Chem* 2020;39:323–334. © 2019 SETAC

Keywords: Methylmercury; Passive sampling; Sediment; Porewater

INTRODUCTION

Mercury is a global pollutant that can be microbially methylated in the environment and biomagnified to levels of concern in human and ecological receptors (Driscoll et al. 2013). Mercury methylation is often localized in redox transition zones near solid–water interfaces (Bigham et al. 2016), making methylmercury (MeHg) readily available for uptake by benthic and epibenthic fauna (Chen et al. 2014). The concentration of chemically labile or bioavailable MeHg (in the present study designated $MeHg_{CL}$) in surface waters and sediment porewaters is needed to make predictions about risk and to evaluate the impact of potential remediation on risk. However, MeHg concentrations can be very low (pM in uncontaminated waters) and highly variable through time, making direct sampling and analysis challenging. The immediate focus of the present study was the development of a passive sampling device that can provide time-averaged concentration trends. Future work is focused on the ultimate goal of predicting MeHg uptake by biota.

Passive samplers have been extensively investigated as a tool to measure freely dissolved concentrations (sometimes designated C_{free}) of other bioaccumulating pollutants, most commonly hydrophobic organic chemicals (HOCs). For HOCs, samplers are made from thin hydrophobic polymer films that allow partitioning and concentration into the polymer matrix. Polymeric samplers for HOCs function as equilibrium samplers, so C_{free} can be calculated based on the known equilibrium partition coefficient between water and the

This article contains online-only Supplemental Data.
* Address correspondence to ughosh@umbc.edu
Published online 6 November 2019 in Wiley Online Library (wileyonlinelibrary.com).
DOI: 10.1002/etc.4631

sampling material for each HOC. Importantly, although C_{free} represents only one of multiple pathways of biotic exposure, its calculation is useful because HOCs are in thermodynamic equilibrium among water, sediment, animal, and sampler compartments (Burgess et al. 2013). This chemical activity–based approach permits the use of equilibrium partitioning coefficients to calculate unknown HOC concentrations as well as to predict the outcome of a perturbation such as the addition of an engineered sediment amendment or an ongoing contaminant input. In this way, porewater passive sampling measurements can serve as a useful proxy for bioavailability (Marvin-DiPasquale et al. 2009; Liu et al. 2012; Amirbahman et al. 2013).

Our goal is to develop a similar approach for MeHg, using the equilibrium model concept developed for HOCs and building on the knowledge gained from passive sampler development for MeHg to date. The best-studied MeHg passive sampler is the diffusive gradient in a thin film (DGT) device (Clarisse et al. 2012; Liu et al. 2012; Amirbahman et al. 2013; Hong et al. 2014; Noh et al. 2016). The DGT samplers are in situ analytical sensors (Davison and Zhang 2012) composed of an inert gel diffusion layer (generally covered by a permeable membrane) over a ligand-bearing resin appropriate to the compound of interest. They are designed to operate as kinetic samplers, in which the amount of metal accumulated depends on the concentration in the external environment, the time of deployment, the rate of diffusion through the gel layer, and the thickness of the gel. They operate as essentially "infinite sinks," meaning that there is a sufficient mass of ligand in the sampler to drive the metal flux from an aqueous phase into the sampler during the entire deployment period (Jiménez Piedrahita 2017). The best-developed DGT samplers for both total Hg and MeHg use thiol-functionalized silica as a ligand, overlaid by either an agarose or a polyacrylamide diffusion layer (Dočekalová and Diviš 2005; Clarisse and Hintelmann 2006; Amirbahman et al. 2013; Lu et al. 2014). One advantage of thiol-based samplers is that they may mimic the dominant MeHg ligands in nature (Zhang et al. 2004; Jeremiason et al. 2015; Liem-Nguyen et al. 2017) and thus potentially provide a good predictor of the flux to aquatic organisms. As a result, site-specific uptake by thiol-based DGT samplers (commonly referred to as C_{DGT} or DGT-labile) has been used to predict Hg availability for methylation (Ndu et al. 2018), de novo MeHg production (Clarisse et al. 2011), MeHg photodegradation rates (Fernández-Gómez et al. 2015), and MeHg uptake by biota (Clarisse et al. 2012; Liu et al. 2012; Amirbahman et al. 2013).

Although DGT samplers for Hg or MeHg were originally developed as a method to estimate freely or total dissolved concentrations in porewater (C_{pw}; Dočekalová and Diviš 2005; Clarisse and Hintelmann 2006; Hong et al. 2014), many studies have recognized that DGT samplers instead access a kinetically labile portion of the total Hg or MeHg pool in sediments (Merritt and Amirbahman 2007; Clarisse et al. 2009; Peijnenburg et al. 2014; Ndu et al. 2018). Thiol-based DGT samplers have generally behaved as predicted by the general form of the DGT mass accumulation equation, with linear Hg and MeHg uptake through several days, although deviations may occur during longer deployment periods (Gao et al. 2011; Clarisse et al. 2012; Amirbahman et al. 2013) or as a result of the deposition of nanoparticles on sampler membranes (Pham et al. 2015). Another potential complication of thiol-based DGT samplers operating as an "infinite sink" for Hg and MeHg is potential perturbation of the local equilibrium among solid and aqueous phases (Peijnenburg et al. 2014), which could lead to overestimation of the chemically or biologically available pool depending on the resupply rate from the solid phase (Clarisse et al. 2011).

One particular challenge in the use of DGT samplers is the choice of diffusion coefficient used for calculation of $MeHg_{CL}$ from $MeHg_{DGT}$ (Noh et al. 2016), which should ideally be consistent across sampling regimes. The distribution of aqueous MeHg forms can vary significantly among environments, and these species occupy a wide range of sizes, diffusivities, and bioavailabilities (Clarisse et al. 2009), greatly increasing uncertainty when extrapolating from DGT to the labile fraction of interest in porewater. For MeHg in typical estuarine and fresh porewaters, the dominant species of $MeHg_{CL}$ are expected to be aqueous complexes with small organic thiols, sulfide, and bulky dissolved organic matter (DOM; Skyllberg 2008; Aiken et al. 2011; Ndu et al. 2015; Liem-Nguyen et al. 2017), as well as the portion of the much larger sediment MeHg pool that is in dynamic equilibrium with aqueous complexes (Benoit et al. 2001; Leaner and Mason 2002). Effective diffusion coefficients range over approximately an order of magnitude between large MeHg–DOM complexes and small MeHg salts for DGT samplers (Clarisse et al. 2009; Hong et al. 2011; Gao et al. 2014). One way around this issue is to use $MeHg_{DGT}$ to directly predict some measure of MeHg bioavailability in a specific environment (Clarisse et al. 2012), but that empirical approach can limit comparison among environments.

By using an equilibrium approach to sampling, our objectives include obviating the use of diffusion coefficients to calculate $MeHg_{CL}$ and limiting perturbation of the dynamic sediment:water equilibrium. Instead, $[MeHg_{CL}]$ can be calculated directly from the measured equilibrium concentration of MeHg in the sampler ($[MeHg_{ps}]$) and the operationally defined partition coefficient between the sampler and its environment (passive sampler–porewater partition coefficient [K_{PW}]):

$$[MeHg_{CL}] = [MeHg_{ps}]/K_{PW}$$

Importantly, the goal of passive sampling efforts is to assess the total pool of labile MeHg. The concentration of $MeHg_{CL}$ will largely be determined by the equilibrium with the large pool of sediment-bound MeHg. If all of the component species of $MeHg_{CL}$ come to equilibrium with the samplers, the concentration of MeHg accumulated in the sampler will reflect $[MeHg_{CL}]$ regardless of MeHg speciation. Thus, the equilibrium concentration of MeHg accumulated in samplers could be used directly to assess MeHg availability. Alternatively, the absolute concentration of $MeHg_{CL}$ can be calculated using the appropriate K_{PW}. In most environments MeHgDOM species are

dominant, so the use of a sufficiently representative, empirically derived K_{PW} for MeHgDOM could be sufficient to determine $MeHg_{CL}$. The advantage of equilibrium passive sampling is that if a standardized sampling material based on cysteine or another sorbent is properly designed, it should approach a steady-state $MeHg_{CL}$ concentration in proportion to steady-state concentrations in benthic animals, irrespective of mechanism (Peijnenburg et al. 2014). The challenges for equilibrium passive sampling are 1) to convincingly demonstrate reversible MeHg equilibrium with the chosen sampler, 2) to establish K_{PW} for environmentally relevant MeHg species, and 3) to evaluate the relevance of sampler data in real sediment systems.

Our approach to developing a novel sampler began by identifying a suite of polymers with affinity for MeHg sufficient to concentrate it to a desirable extent but without dramatically exceeding native sediment–water partitioning (K_d). For our purposes, this entailed a target range for logarithmic passive sampler–water linear partitioning constants (log K_{PW}) of 3.0 to 4.5. This range was also selected in part to ensure accumulation of detectable masses of MeHg in a reasonably sized sampler, without causing local depletion of $MeHg_{CL}$ through the addition of a small mass of high-affinity ligand in the sampler material. More than 30 materials were screened in isotherms for MeHg complexed with either HO^- or Suwannee River humic acid (HA), ligands chosen to bracket a range of size and lability for relevant MeHg species. Some of the most successful materials were chosen to proceed to further, more environmentally realistic tests, first in slurried soils and sediments and then in stagnant sediment microcosms. One particularly promising material, an agarose gel containing suspended activated carbon (AC) particles, was subjected to additional experiments to investigate its kinetics of MeHg uptake and release. Several of the other materials we tested also demonstrated desirable MeHg partitioning and remain candidates for future development. The present study represents a proof of concept for equilibrium MeHg passive sampling and sets the stage for further work toward the ultimate goal of enabling reproducible measurements of bioavailable $MeHg_{CL}$ and improving risk assessment and management for mercury-contaminated sites.

MATERIALS AND METHODS

Material selection and preparation

The potential passive sampling materials tested in the present study fall under 3 categories: 1) standard laboratory polymers not specifically designed for metal sorption, 2) polymers containing AC, and 3) polymers with reduced sulfur chemical functionality. Agarose gels were prepared with an existing method (Gao et al. 2011), but suspensions of sorbents in agarose were based on custom formulations. Sulfur-functionalized polymers were identified in the biomedical (Bernkop-Schnürch et al. 2001; Duan and Lewis 2002; Bhalekar et al. 2013) or water treatment (Yu et al. 2012) literature. A method for embedding AC in a polyvinylidene fluoride (PVDF) polymer was adapted from an electrochemistry application (Choi 2010). A complete list of 30 tested samplers and references to preparation methods is presented in Table 1, and photographs of selected samplers appear in Supplemental Data, Figure S1. For all experiments except initial screening isotherms, agarose gels were prepared with uniform thickness (800 μm except where noted) by casting between glass plates separated by spacers. Spacer and gel thicknesses were verified with a 0 to 1″ digital micrometer (iGaging).

Screening isotherms

MeHgOH isotherms. Small (~1–5 cm on a side) pieces of test material were cleaned, dried, weighed, and placed in 60-mL polyethylene terephthalate glycol (PETG) copolymer bottles containing 50 mL deionized water adjusted to 3 ppt salinity with Instant Ocean® (Spectrum Brands Pet). All experiments were run at low salinity for consistency and to mimic the conditions at our primary field site, an oligohaline, estuarine marsh. In this experiment, $[Cl^-]$ was sufficiently low and pH sufficiently high (~9 as predicted by MINEQL and verified by direct measurement) that MeHg was predominantly complexed with HO^- rather than Cl^-. The solutions were spiked with MeHg at concentrations ranging from 3 to 300 ng L^{-1} (unmodified polymers) or 30 to 3000 ng L^{-1} (modified polymers). These were chosen in consideration of analytical detection limits and anticipated partitioning. Samples were incubated for 14 d in the dark at 4 °C with orbital shaking at 120 rpm. Following incubation, sample waters were passed through 0.45-μm GD/X filters (Whatman; glass microfiber in propylene housing) with disposable plastic syringes. Filtrates were processed and analyzed for MeHg. In screening isotherms only, the mass-normalized sampler concentration, C_{ps}, was calculated from the difference between spiked and recovered MeHg in water. In all other experiments, samplers were directly distilled and analyzed. Sampler–water partitioning coefficients, K_{PW}, were calculated from linear regression fitting of C_{ps} and C_w to an isotherm model. Control bottles with no sampler were used to assess loss of MeHg to degradation or sorption to bottle walls. Fractional losses in control bottles were inversely related to initial spike concentrations, such that partitioning by unmodified samplers could have been somewhat underestimated at low spike levels. However, losses were negligible at the higher concentrations used for actual samplers containing AC or sulfhydryl functionality.

MeHg Suwannee River HA isotherms. We also evaluated partitioning of MeHg complexed with Suwannee River HA (MeHgSRHA) to several samplers. Isotherms were set up as in the MeHgOH isotherms but with the addition of SRHA Standard II (International Humic Substances Society) in a 10^6:1 SRHA:MeHg mass ratio in each sample and 7.5 mM $NaHCO_3$ to buffer pH at 8. A high SRHA:MeHg mass ratio was chosen to avoid saturating thiolic sites, which control MeHg complexation with DOM under normal environmental conditions (Haitzer et al. 2002). To ensure a stable MeHg distribution, solutions were incubated overnight after addition of SRHA but before the addition of samplers. The assumption of an

TABLE 1: Summary of materials screened in methylmercury (MeHg) isotherm experiments[a]

Abbreviation	Material	Target sorbent concentration	MeHgOH		MeHgSRHA	
			Log K_{PW}[b]	p	Log K_{PW}[b]	p
AC	Activated carbon	n/a	5.22 ± 0.49	0.0004	n.d.	n.d.
ag	Agarose	n/a	2.06 ± 0.44	0.0018	n.d.	n.d.
ag+AC	Activated carbon suspended in agarose	10% w/w AC	3.46 ± 0.07	0.0004	2.81 ± 0.20	0.0008
ag+Cys	L-Cysteine dissolved in agarose	2% w/w Cys	3.07 ± 0.33	0.0025	n.d.	n.d.
ag+Cys-alg	L-Cysteine-functionalized alginate suspended in agarose	5% w/w Cys	3.26 ± 0.24	0.0009	n.d.	n.d.
ag+Cys-xylo	L-Cysteine-functionalized xyloglucans suspended in agarose	5% w/w Cys	3.03 ± 0.40	0.0047	n.d.	n.d.
ag+MAA-chit	Mercaptoacetic acid–functionalized chitosan suspended in agarose	0.3% w/w mercapto	3.01 ± 0.22	0.0009	n.d.	n.d.
ag+MPTMS-DE	(3-Mercaptopropyl)trimethoxysilane-functionalized diatomaceous earth suspended in agarose	1% w/w mercapto	3.39 ± 0.64	0.0132	2.97 ± 0.12	0.0001
ag+SAMMS	Thiol-SAMMS suspended in agarose	2% w/w SAMMS	5.19 ± 0.25	0.0002	3.01 ± 0.37	0.0040
agPEG	Agarose doped with polyethylene glycol and glycerol	n/a	2.17 ± 0.13	0.0367	n.d.	n.d.
agPEG+AC	Activated carbon suspended in polyethylene glycol–doped agarose	3% w/w AC	3.28 ± 0.12	0.0001	2.87 ± 0.37	0.0045
agPEG+SAMMS	Thiol-SAMMS suspended in polyethylene glycol–doped agarose	2% w/w SAMMS	3.89 ± 0.02	<0.0001	3.02 ± 0.20	0.0006
CA	Cellulose acetate	n/a	2.37 ± 0.20	0.0072	n.d.	n.d.
CA+MA	Mercapto-functionalized cellulose acetate	20% w/w mercapto	2.43 ± 0.12	0.0002	n.d.	n.d.
CN	Cellulose nitrate	n/a	2.99 ± 0.08	0.0006	n.d.	n.d.
DE	Diatomaceous earth	n/a	2.55 ± 0.18	0.0007	n.d.	n.d.
MPTMS-DE	Mercapto-functionalized diatomaceous earth	3% w/w mercapto	5.82 ± 0.43	0.0009	n.d.	n.d.
Parafilm	Paraffin	n/a	2.14 ± 0.21	0.0019	n.d.	n.d.
PDMS	Polydimethylsiloxane	n/a	1.82 ± 0.23	0.0158	n.d.	n.d.
PES	Polyethersulfone	n/a	2.44 ± 0.43	0.0107	n.d.	n.d.
PET+Cys	L-Cysteine-functionalized polyethylene terephthalate	8 nmol Cys cm^{-2}	3.14 ± 0.32	0.0022	2.82 ± 0.28	0.0021
POM38	Polyoxymethylene (38 μm thick)	n/a	1.80 ± 0.34	0.0343	n.d.	n.d.
PTFE	Polytetrafluoroethylene	n/a	1.82 ± 0.17	0.0016	n.d.	n.d.
PVDFm+AC	Activated carbon suspended in PVDF prepared with 1:1 methanol:water nonsolvent	10% w/w AC	3.73 ± 0.60	0.0248	n.d.	n.d.
PVDFw	Polyvinylidene fluoride prepared with water nonsolvent	n/a	2.11 ± 0.16	0.0009	n.d.	n.d.
PVDFw+AC	Activated carbon suspended in PVDF prepared with water nonsolvent	10% w/w AC	3.16 ± 0.17	0.0003	2.82 ± 0.34	0.0036
PVDFw+Cys	L-Cysteine dissolved in PVDF	6% w/w Cys	4.11 ± 0.32	0.0010	n.d.	n.d.
PVDFw+SAMMS	Thiol-SAMMS suspended in PVDF	5% w/w SAMMS	3.86 ± 0.29	0.0009	2.99 ± 0.21	0.0008
SAMMS	Thiol-SAMMS	n/a	5.63 ± 0.62	0.0028	n.d.	n.d.

[a]Experimental data fit to a linear isotherm model.
[b]Partition coefficient ±1 standard error.
References or sources for polymers and sorbents: ag, Gao et al. (2011); Cys+alg, Bernkop-Schnürch et al. (2001); Cys+xylo, Bhalekar et al. (2013); ag+MAA-chit, Kast and Bernkop-Schnürch (2001); ag+MPTMS-DE, Yu et al. (2012); SAMMS, Steward Environmental Solutions; agPEG, Charlionet et al. (1996); CA, Membrane Filtration Products; MA, Aoki et al. (2007); CN, Membrane Filtration Products; DE, Honeywell; MPTMS-DE, Yu et al. (2012); parafilm, Bemis; PDMS, Altec; PES, Goodfellow Cambridge; PET+Cys, Duan and Lewis (2002); POM38, CS Hyde; PTFE, Grainger.
K_{PW} = sediment–porewater partition coefficient; n/a = not analyzed; n.d. = not determined; SRHA = Suwannee River humic acid.

overnight equilibrium between MeHg and SRHA was based on the work of Luengen et al. (2012). Isotherm results for all tested materials can be found in Table 1.

Sampler kinetics and mechanism of accumulation

In an initial range-finding experiment, 2 samplers, an agarose gel with embedded AC particles (ag+AC) and a polyethylene terephthalate sheet covalently modified with cysteine residues (PET+Cys), were exposed to MeHgOH or MeHgSRHA solutions for 7 h or 1, 7, 14, or 28 d. Solutions were sampled destructively at each time point, and water filtrates and samplers were processed and analyzed for MeHg.

In a subsequent experiment, pieces of ag+AC of identical composition but contrasting thicknesses (0.80 × 5 × 5 mm vs 0.17 × 10 × 10 mm) were exposed to MeHgSRHA to determine whether it diffuses into the sampler or is restricted to surface adsorption. A solution of 3 ppt Instant Ocean, 7.5 mM $NaHCO_3$, and 5 mg L^{-1} SRHA was prepared and passed through a 0.7-μm AQFA filter. The filtrate was spiked to 50 ng L^{-1} MeHg and allowed to equilibrate overnight before being apportioned to exposure bottles. Samplers were added to bottles and exposed in the dark at 4 °C with orbital shaking at 60 rpm. Samples were collected destructively after 6 min, 2.4 h, 7 h, 1 d, 3 d, 7 d, 21 d, and 58 d. Waters and samplers were collected, preserved, and analyzed. Results from the 21- and 58-d time points are not reported because C_w had dropped substantially in both sampler and control bottles as a result of MeHg degradation.

To evaluate the effects of DOM concentration on MeHg accumulation of target sampler sorbent materials, uptake

of MeHgSRHA onto granular AC and granular thiol–self-assembled monolayers on mesoporous supports (SAMMS) was investigated. Solutions of MeHgSRHA, 20 mL, were prepared at DOM concentrations ranging from 5 to 500 mg L^{-1}, with MeHg added to reach an initial concentration of 500 ng L^{-1}. Similar to the isotherm experiments, bottles were incubated overnight in the dark at 4 °C with orbital shaking at 60 rpm to ensure equilibrium between MeHg and SRHA. Approximately 10 mg of granular sorbent material was then added to each bottle, and bottles were exposed for 2 d in the dark at 4 °C with orbital shaking at 60 rpm. Waters and sorbent materials were collected after separation by centrifugation, preserved, and analyzed. Each experimental treatment was conducted in triplicate.

AC kinetics and desorption

To improve our understanding of the nature of accumulation by AC-based samplers, we investigated the kinetics of mercury sorption to AC. Granular AC (Calgon Type 3055; 80 × 325 TOG LF, Chemical Abstracts Service no. 7440-44-0, sieved to >53 μm prior to use) was weighed into PETG bottles containing 50 mL of deionized water with 3 ppt Instant Ocean and 5000 ng L^{-1} Hg or 250 ng L^{-1} MeHg. Control bottles without AC contained 50 ng L^{-1} Hg or 20 ng L^{-1} MeHg. Initial spikes were based on anticipated final concentrations and analytical detection limits. Bottles were incubated for 5 min, 30 min, 6 h, or 2 d, after which shaking was halted and AC particles were allowed to settle. Waters were carefully removed by pipet while minimizing withdrawal of AC, filtered, preserved, and analyzed. To measure desorption from AC, a fresh solution without mercury spike was added to the original exposure bottles up to the 50-mL mark, and the bottles were incubated for the same amounts of time as in the exposure step. Bottle weights were collected before and after each step to track solution volumes, and exposure times were recorded to the minute. Each adsorption and desorption time point was run in duplicate (controls) or triplicate (AC).

Soil and sediment slurries

A natural soil and sediment were used to test the predictive capabilities of select samplers in more complex and environmentally realistic chemical matrices encompassing a range of MeHg concentrations. Soil from the upper 15 cm of a Berry's Creek (Bergen County, NJ, USA) *Phragmites* tidal marsh was collected in June 2015 in a location containing approximately 50 ppm total Hg and 25 ppb MeHg. Estuarine sediment was collected from the Rhode River dock at the Smithsonian Environmental Research Center in Edgewater, MD, USA. It contained approximately 0.1 ppm solid-phase Hg and <5 ppb MeHg. Initial sediment and soil chemistry can be found in Supplemental Data, Table S1. Slurries of each were prepared with degassed, deionized water containing 3 ppt Instant Ocean in a 9:1 weight ratio with solids. All subsequent handling was performed in an anaerobic glove bag. Slurries were spiked with unlabeled Hg equal to 10% (soil) or 20% (sediment) of the native, dry-weight Hg content to encourage additional MeHg formation. Slurries were incubated for 7 d with a gentle shake once per day before apportionment to sample jars. Three sampler types were tested in duplicate: ag+AC, an agarose suspension of the engineered sorbent material thiol-SAMMS (ag+SAMMS), and PET+Cys. Samplers (~5–25 cm on a side) were cleaned, dried, weighed, measured, and placed in small baskets prepared by folding strips of polypropylene mesh and sewing edges together with nylon thread (Supplemental Data, Figure S1c). Mesh and thread were washed with 1 M HNO_3, followed by deionized water prior to use. Samplers in baskets were placed in wide-mouth, glass sample jars containing 50 mL equilibrated soil or sediment slurry. Two additional "canary" jars of each slurry were prepared without samplers but with 2 mg L^{-1} resazurin to monitor redox status. Jars were kept on ice for 20 d to minimize further MeHg production and gently swirled once per day. After exposure, samplers were removed from jars and baskets, gently rinsed with deionized water, blotted with laboratory wipes, weighed, and frozen. An aliquot of overlying water was collected from each jar for pH measurements, and the remaining jar contents were transferred to tubes and centrifuged at 4200 rpm for 7 min. Supernatants were passed through 0.45-μm glass microfiber syringe filters with disposable plastic syringes into clean, 60-mL PETG bottles. Aliquots were set aside for analysis of sulfide and dissolved organic carbon (DOC). Remaining filtrates were acidified with 0.5% HCl and refrigerated, then processed and analyzed for MeHg, sulfide, and pH (Supplemental Data, Table S2). Pelleted solids were lyophilized and weighed repeatedly until weights were replicable, then processed and analyzed for MeHg.

Static sediment microcosms

In a further step toward simulating realistic deployment conditions, samplers were tested in static sediment microcosms. Bottom sediment was collected to a depth of 15 cm from a tidal creek in the upper part of Berry's Creek. The sediment was silty mud with solid-phase Hg concentrations of 40 to 50 ppm. Sediments were collected in May 2016 in 5-gallon buckets, shipped on ice to the Smithsonian Environmental Research Center, and maintained at 4 °C until the start of the experiment in August. Sediments were mixed by hand, and a portion was amended with 5 wt% AC. For microcosms, 200 g sediment with or without AC was combined with 225 mL overlying water (5 ppt Instant Ocean) in 800-mL plastic beakers. Beakers were loosely lidded, gently aerated, and kept at room temperature (Supplemental Data, Figure S2). Microcosms equilibrated 14 d prior to sampler insertion to allow redevelopment of a vertical redox gradient. In each beaker, one ag+AC sampler in a protective basket was fully submerged in the uppermost 0.5 cm of sediment, spanning the visually apparent redox transition zone. To assess kinetics of uptake, samples were collected destructively at 0, 8, 14, 21, and 28 d of exposure. Samplers were removed from baskets, preserved, and analyzed as before. Sediment and porewater were

separated by centrifugation at 4000 rpm for 5 min and handled as in the slurry experiment. Sediment and porewater measurements reflected vertical averages of the entire depth of sediment in the microcosms (2–3 cm). Overlying water was gently replaced in the remaining beakers on sampling days.

Analytical methods

In all matrices MeHg was measured by isotope dilution mass spectrometry after separation and cleanup by distillation (Gilmour et al. 2013). Total Hg was also measured using isotope dilution inductively coupled plasma mass spectrometry (ICP-MS) following $SnCl_2$ reduction to Hg^0. Water samples were digested with BrCl and sediment samples with 7:4 HNO_3:H_2SO_4. Further details and quality assurance data are found in the Supplemental Data, including Table S3.

Equilibrium speciation calculations

The chemical modeling program MINEQL+ v.4.6 (Environmental Research Software) was used to calculate equilibrium aqueous MeHg speciation in all experimental systems. Conditional stability constants for a variety of MeHg complexes were obtained from literature sources and added to the software's database, as outlined in Supplemental Data, Table S4. All other thermodynamic constants were software defaults.

RESULTS AND DISCUSSION

Screening isotherms

MeHgOH isotherms. As shown in Table 1, initial isotherm tests demonstrated greatly enhanced sorptive capabilities of both AC- and thiol-modified polymers relative to unmodified hydrophobic polymers and permitted the selection of a subset of enhanced polymers to proceed to subsequent tests. Partitioning of MeHgOH by 8 unmodified hydrophobic polymers was generally well below our target range for linear partitioning log K_{PW} of 3.0 to 4.5. This outcome was to be expected given the low hydrophobicity of MeHgOH (log $K_{PW} = -1.2$ [Mason 2001]). By contrast, partitioning of MeHgOH into many of the AC- and thiol-modified polymers fell comfortably within our target range, and sorption isotherms remained mostly linear over multiple orders of magnitude, as shown for 3 selected polymers in Figure 1A (log-transformed data) and for all 28 polymers in Table 1. Linear isotherms for MeHg on AC at low environmentally relevant concentrations have been published by others (Gomez-Eyles et al. 2013). We also fitted partitioning data to Freundlich isotherms and found Freundlich parameters ($1/n$) <1 for some samplers (Supplemental Data, Table S5). However, curves only diverged from linearity at unrealistically high C_w (Supplemental Data, Figure S3) for most samplers, so reported K_{PW} values represent the regression fitted values for linear isotherms. Isotherm results were compared to the partitioning expected based on the composition of the samplers. This analysis revealed that some of the samplers permitted relatively free diffusion of MeHgOH, whereas

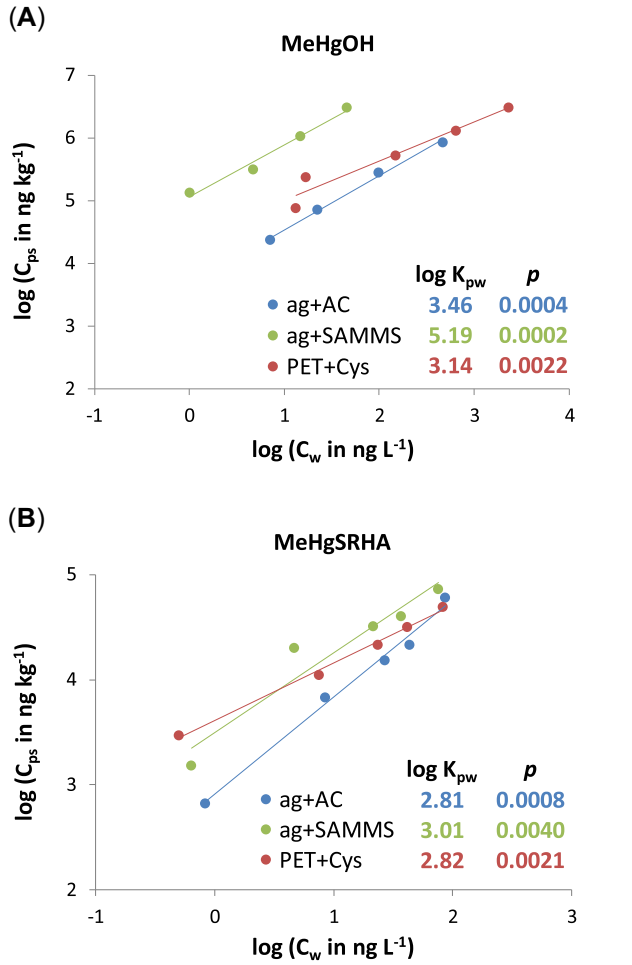

FIGURE 1: Partitioning of (**A**) methylmercury (MeHg)OH and (**B**) MeHg Suwannee River humic acid (SRHA) to select samplers in 14-d aqueous isotherm tests. Note different axis scales. AC = activated carbon; ag = agarose; Cys = cysteine; K_{PW} = sediment–porewater partition coefficient; PET = polyethylene terephthalate; SAMMS = self-assembled monolayers on mesoporous supports.

others were diffusion-limited (i.e., measured partitioning was much lower than predicted). A detailed discussion of sampler permeability is found in the Supplemental Data, and supported by Table S6.

Three samplers, ag+AC, ag+SAMMS, and PET+Cys, were identified as the most promising based on the strength and proportionality of their partitioning and their physical attributes. The sulfur-functionalized biomedical polymers ("thiomers")—including thiolated chitosan and cysteinylated alginate and xyloglucans—lacked mechanical strength as prepared and were suspended in agarose to confer stability in isotherm tests. Though they also partitioned well, they were excluded from further consideration because of the additional complexity involved in their preparation and the availability of several viable alternatives. ag+MPTMS-DE, an agarose gel containing (3-mercaptopropyl)trimethoxysilane-modified diatomaceous earth, performed well in isotherm tests but was not carried forward because of sample size limitations. This material remains a good candidate for future investigation.

MeHgSRHA isotherms. Partitioning of MeHgSRHA was reduced compared to MeHgOH for all tested samplers (Figure 1B). Speciation modeling for isotherms run with added SRHA predicted virtually complete complexation of MeHg with SRHA. Compared to smaller MeHg complexes, MeHg complexed with DOM is both less diffusive and less bioavailable (Choi et al. 1998; Fernández-Gómez et al. 2014). This experiment therefore represents an important contrast to the idealized scenario in the previous set of isotherms. However, in all cases partitioning remained in or near our target range and was proportional across a range of C_w ($r^2 \geq 0.93$). The lowest K_{PW} was measured for ag+AC. Under true, diffusively unconstrained equilibrium conditions, the extent of MeHg partitioning to AC particles should theoretically be the same irrespective of the other ligands present. That this did not occur suggests that the MeHgSRHA–AC interaction may have effectively reflected an SRHA–AC interaction with MeHg incidentally associated, a hypothesis we confirmed in a separate study (Schwartz et al. 2019).

The size of the decrease in K_{PW} from MeHgOH to MeHgSRHA varied among samplers, possibly reflecting differences in their physical structures and uptake mechanisms. For example, the K_{PW} decrease was relatively small for PET+Cys, a sampler with readily accessible binding sites on its surface and presumably not limited by diffusion. By contrast, the decrease was more pronounced for ag+SAMMS, which requires diffusion through both agarose and thiol-SAMMS, a highly structured material with pore sizes on the order of 2 to 20 nm (Pacific Northwest National Laboratory 2009). Methylmercury complexed with SRHA, which forms colloids in the range of 0.5 to 2 nm and aggregates to some extent, may be less readily accessible to such a sampler (Balnois et al. 1999; Hosse and Wilkinson 2001). Fouling of thiol-SAMMS by SRHA may also have contributed to lower-than-predicted MeHg uptake. Despite these differences, the generally positive results for several samplers in both the MeHgOH and MeHgSRHA isotherms were encouraging and indicated their potential to function across a variety of water chemistries and MeHg species.

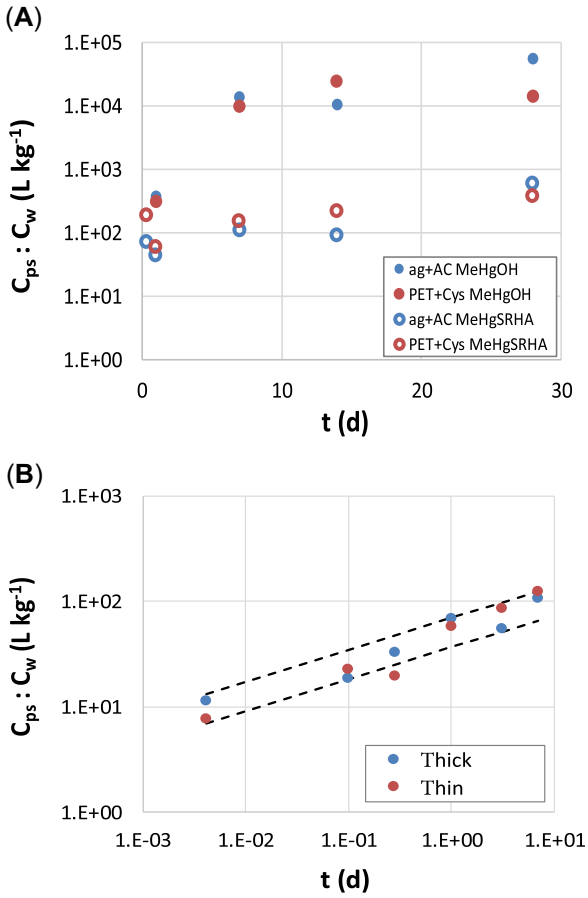

FIGURE 2: (**A**) Kinetic curves for polymer–water partitioning of methylmercury (MeHg)OH (filled circles) and MeHg Suwannee River humic acid (SRHA; open circles) by ag+AC (blue) and polyethylene terephthalate (PET) + cysteine (Cys; red). Note arithmetic versus logarithmic axes. (**B**) Kinetic curves for partitioning of MeHg SRHA by ag+AC with 2 contrasting surface area-to-volume ratios: 3.3 mm^{-1} ("thick," blue) and 12.2 mm^{-1} ("thin," red). Dotted lines: upper and lower 95% confidence intervals for power fit of thick data. In both figures, each point represents $n = 1$. AC = activated carbon; ag = agarose.

Sampler kinetics and mechanism of accumulation

In a range-finding kinetics experiment in aqueous solution, both ag+AC and PET+Cys approached equilibrium partitioning of MeHgOH after 2 wk (Figure 2A; Supplemental Data, Table S7). For both sampler types, the uncertainty ranges in log K_{PW} from the isotherm experiment overlap with the 95% confidence intervals at the 14-d point in this experiment (based on linear regression of log-transformed partitioning vs time). Absolute accumulation of MeHgSRHA was depressed compared to MeHgOH, with lower partitioning at each time point. The shape of the MeHgSRHA kinetic curve was also flatter, making equilibration difficult to verify.

In addition to kinetics, the mechanisms of MeHg accumulation by samplers are an important consideration in sampler development. An understanding of where and how sorption occurs is required to interpret sampler concentrations and optimize form factors. Polyethylene terephthalate is a relatively impermeable polymer, so both the cysteinylation of PET and the accumulation of MeHg by PET+Cys can be assumed to occur mostly on the sampler's surface. By contrast, agarose is permeable and readily permits diffusion of MeHg even in the presence of DOM (Fernández-Gómez et al. 2014). To verify a permeation-based mechanism of accumulation by ag+AC, pieces of the material with contrasting surface area-to-volume ratios were exposed to aqueous MeHgSRHA and sampled along a time course. If internal diffusion were substantially inhibited relative to diffusion to sampler surfaces, accumulation would increase with increasing surface area-to-volume ratio. However, this was not the case. Aside from one point, the uptake curves of the 2 thicknesses were indistinguishable (power fit, $p = 0.05$; Figure 2B; see Supplemental Data, Table S8, for mass balance data). This strongly suggests that even large MeHg complexes (MeHgSRHA has an average molecular weight of 1399 daltons [Waples et al. 2005]) readily permeate the agarose matrix of ag+AC, in contrast to PVDF

(see discussion of sampling mechanisms in Supplemental Data). A simple modeling exercise supports this contention. The diffusion coefficient (D) in agarose of MeHg complexed with DOM from a Nordic reservoir is 2.68×10^{-6} cm^2 s^{-1}, only 15% lower than that of MeHg without DOM (Fernández-Gómez et al. 2014). Assuming that this value of D is similar to that of MeHgSRHA, a Fickian diffusion calculation predicts >90% equilibration by agarose within 1 d at a depth of 400 µm (the half-thickness of our sampler). For comparison, our kinetic curves indicate an approach to equilibrium over several days to a week or more. It should also be borne in mind that the average pore size in our agarose gels, though not directly measured, is probably approximately 400 nm (Pernodet et al. 1997), whereas SRHA would have been on the order of 1 nm (Balnois et al. 1999) and subject to only limited aggregation (Hosse and Wilkinson 2001). These considerations suggest that both the kinetics and equilibrium partitioning capacity of ag+AC are controlled by the included AC particles and not the agarose gel. This opens the possibility of tuning the sampler's performance by adjusting the concentration and properties of the AC or other sorbents used in its formulation. In addition, there is an opportunity to design the polymer matrix to exclude the diffusion of DOM-bound MeHg if necessary.

An experiment was conducted to understand the effect of DOM on the accumulation of MeHg species by the target sorbent materials. A gradient of SRHA concentrations was chosen to represent environmentally relevant DOM concentrations (5–50 mg L^{-1}), as well as a DOM concentration elevated above what would be expected in most environments (500 mg L^{-1}). Partitioning of MeHgSRHA to bare AC particles exhibited relatively consistent values across the environmentally relevant DOM gradient (log K_{AC} 3.77–3.35). Similarly, partitioning of MeHgSRHA to bare thiol-SAMMS was relatively consistent across the same range (log K_{SAMMS} 4.30–4.26; Supplemental Data, Table S9). Both sorbents exhibited decreased partitioning of MeHgSRHA at elevated DOM concentrations (500 mg L^{-1}). This behavior suggests that over environmentally relevant DOM concentration ranges, even in field deployments with fluctuating DOM concentrations, both of these tested sorbent materials will provide reasonable estimates of MeHg C_{pw} when using the empirically determined K_{PW} for these materials.

AC kinetics and desorption

A separate experiment was performed to characterize adsorption onto and desorption from bare AC particles. Partitioning of MeHgOH to AC was rapid (Figure 3; Supplemental Data, Figure S4), approaching the previously published log K_{AC} value of 4.89 within 5 h and slightly surpassing it (5.01–5.21, $n = 3$) by 2 d (Gomez-Eyles et al. 2013). A model fit of MeHg adsorption is shown in Supplemental Data, Figure S4b. When MeHg-loaded AC was exposed to clean water, reequilibration to a similar log K_{AC} (5.00–5.22, $n = 3$) occurred within 3.6 h (shown in Figure 3; details in Supplemental Data, Table S10). Because complete removal of the original exposure solutions was impossible without also removing AC, some MeHg-spiked water (usually ~2 mL) carried over into the 50-mL desorption solutions. However, the masses of MeHg released from AC exceeded the masses carried over, and MeHg in water increased with desorption time, confirming that MeHg indeed desorbed from AC. Carryover MeHg accounted for 15 to 30% of the totals measured in water after desorption. These findings support the notion of a reversible, relatively rapid equilibrium between AC and MeHg in water and, by extension, between ag+AC and MeHg in water. Thus, in a field deployment, the sampler would report not the maximum concentration detected but rather an integration of the ambient concentrations experienced throughout the exposure. The dimensions of the sampler and AC particles could be manipulated to achieve a desired timescale for exchange.

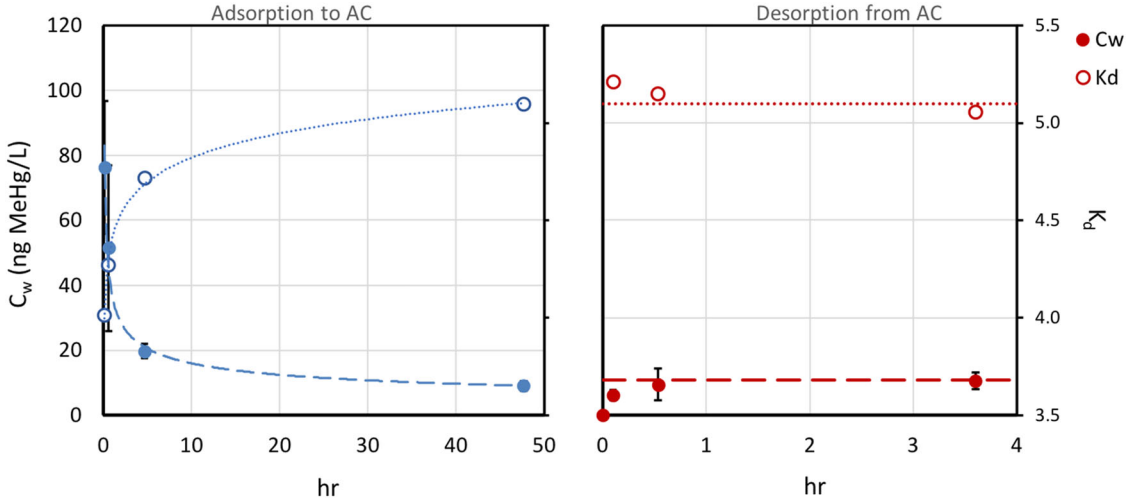

FIGURE 3: Kinetics of methylmercury (MeHg)OH adsorption to a coal-derived activated carbon (AC; initial $C_w = 250$ ng L^{-1}) and desorption of MeHg after transfer to water containing no initial MeHg. Concentrations of MeHg in water over time are shown as filled circles; error bars show ±1 standard error. Partitioning coefficients (K_d) for MeHg to AC are shown with open circles. For the adsorption phase, dashed lines represent logarithmic best fit line; for the desorption phase, dashed lines represent final values observed during the adsorption phase.

Adsorption and desorption of Hg_i were also rapid. The previously reported K_{AC} of 6.55 (Gomez-Eyles et al. 2013) was attained (6.63–6.77, $n = 3$) within 30 min, and a similar value (6.13–6.64, $n = 2$) was measured after just 36 min of desorption in clean water. The model fit produced a higher rate constant and equilibrium concentration compared to MeHg (Supplemental Data, Figure S5 and Table S11).

The kinetics of sorption by porous media are characterized by multiple mechanistic steps, including diffusion to sorbent surfaces and intraparticle diffusion (Boyd et al. 1947). Given the shape of the kinetic curve for MeHg on bare AC particles, it is reasonable to assume that, for ag+AC in our well-mixed systems, intraparticle diffusion was rate-limiting at later time points. However, in a passive sampler deployment in stagnant sediment, diffusion to the sampler's surface would be slower and would exert a greater impact on overall rate. In that case, equilibration could be slower (Mohan et al. 2001). Further work is needed to understand the kinetics of sorption by samplers relative to those of MeHg ligand exchange in porewater and, for sulfur-based samplers, at sorbent sites.

Soil and sediment slurries

In the more chemically complex and realistic milieu of slurries, all 3 tested sampler types successfully predicted MeHg C_{pw}, giving an early indication that they may be viable for use in field conditions (Figure 4). All samplers were retrieved intact after 20 d of exposure. The 2 experiments, using an uncontaminated estuarine sediment (Rhode River) and a contaminated marsh soil (Berry's Creek), provided a test across sharply contrasting porewater MeHg concentrations and speciation. Redox conditions in the Rhode River sediment slurries, as indicated by a resazurin color change in the canary jars and low (<1 μM) sulfide concentrations throughout the experiment, did not favor MeHg production (Supplemental Data, Tables S1 and S2). As a result, aqueous MeHg concentrations at the end of the exposure were extremely low (0.12 ± 0.043 ng L^{-1}). Both aqueous and sampler MeHg measurements were close to method detection limits (Supplemental Data, Table S3) and highly variable (one outlying value was excluded for failing a Dixon's *Q* test). In comparison, the Berry's Creek soil slurry porewaters were initially strongly reducing with high sulfide concentrations (269 ± 1.96 μM), although slurries became less reducing over the course of the exposure study, with porewater sulfide declining to <1 μM by the end of the exposure. The contrast in redox status drove a change in MeHg speciation. Modeling results for the Berry's Creek soil slurries indicated that MeHgSH predominated at day 0 but by day 20 the balance had shifted to complexes with DOM. (In Rhode River sediment slurries, DOM complexes predominated at both time points.) No color change was observed in the corresponding Berry's Creek soil canary jars. Despite the change in redox conditions, final aqueous concentrations of MeHg were considerably higher than in Rhode River slurries (8.7 ± 1.5 ng L^{-1}), permitting more reproducible measurements of both water and samplers.

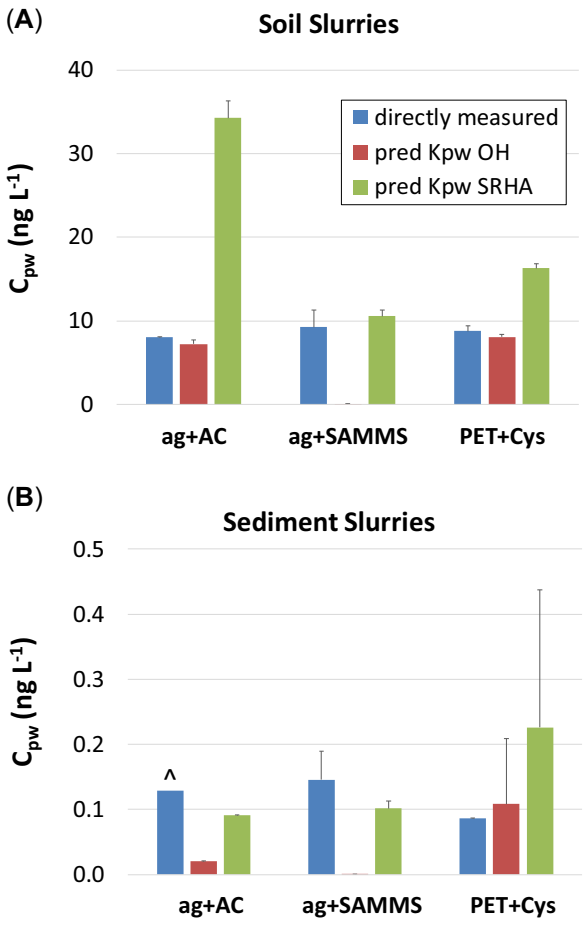

FIGURE 4: Porewater methylmercury (MeHg) concentrations in (**A**) slurried soil and (**B**) sediment. Blue bars = directly measured in centrifuged porewater; red bars = predicted by applying measured polymer concentrations (C_{ps}) to linear fit from MeHgOH isotherm experiment. Green bars = predicted by applying C_{ps} to linear fit from MeHg Suwannee River humic acid (SRHA) isotherm experiment. Error bars show +1 standard error ($n = 2$ except ^, $n = 1$). Note different axis scales. In (**B**), lower detection limits were 0.05 to 0.13 ng L^{-1} for porewater and 1.03 to 92.16 ng kg^{-1} for samplers. ag = agarose; Cys = cysteine; K_{PW} = sediment–porewater partition coefficient; PET = polyethylene terephthalate; SAMMS = self-assembled monolayers on mesoporous supports.

To contextualize these results, we used sampler accumulation in slurries in combination with partitioning coefficients generated in screening isotherms to calculate "predicted" C_{pw} in slurries. Figure 4 presents a comparison of the directly measured concentrations in centrifuged porewater with sampler-predicted values using K_{PW} obtained from independent MeHgOH and MeHgSRHA isotherms. The accuracy and replicability of sampler predictions were greater in Berry's Creek soil slurries, where both porewater and sampler concentrations were further above analytical detection limits. In general, sampler predictions based on MeHgSRHA K_{PW} values agreed with direct measurements in both Rhode River and Berry's Creek slurries. Predictions were within a factor of 2 in 4 cases and within a factor of 4 in the remaining 2. There was greater underprediction based on MeHgOH K_{PW} values. This is

unsurprising given that porewater speciation was dominated by DOM. Thus, for accurate estimation of the total dissolved concentration of MeHg, it is important to use the K_{PW} value corresponding to the dominant MeHg species. In the present study we measured sampler K_{PW} for 2 of the most common MeHg ligands. Additional work is needed for predictions where HS^- or Cl^- may represent the dominant complexing ligand. We hypothesize that K_{PW} for MeHgCl will be similar to K_{PW} for MeHgOH, but partitioning of the bisulfide complex is more difficult to predict. Measured log K_{PW} values in Berry's Creek soil slurries (based on filtered porewater measurements) were 3.41 (ag+AC), 3.12 (ag+SAMMS), and 3.11 (PET+Cys), all within our target range and close to the independently measured K_{PW} values in MeHgSRHA isotherms. It should be emphasized that sampler measurements are time-integrative, whereas direct measurements represent snapshots of porewater concentrations. As such, some differences between the 2 are to be expected.

Static sediment microcosms

As they did in well-mixed soil slurries, ag+AC samplers calibrated with K_{PW} for MeHgOH again made good predictions of MeHg concentrations in estuarine sediment porewater, here at low C_{pw} and under stagnant, poorly mixed conditions (Figure 5). Directly measured C_{pw} in unamended sediment collected from a different Berry's Creek location was 1.7 to 3.7 ng L^{-1} across the duration of the experiment. The C_{pw} predicted by samplers using K_{PW} from Berry's Creek soil slurries was 1.7 to 4.6 ng L^{-1}, statistically indistinguishable from direct measurements at each of the 4 time points (*t* test, $\alpha = 0.05$). The slurry K_{PW} was deemed most applicable because modeled MeHg speciation was similar in the 2 experiments (i.e., dominated by complexes with Berry's Creek DOM). The samplers' consistently accurate measurements across 2 experiments were notable. Interestingly, despite the modeled dominance of DOM complexes, better C_{pw} predictions were obtained from ag+AC using its isotherm K_{PW} for MeHgOH than for MeHgSRHA. This could be attributable to differences between SRHA and the DOM native to these estuarine sediments. Suwannee River HA is a terrestrially derived DOM occupying the high range of both aromaticity and molecular weight and may also have a greater density of thiol sites compared to DOM native to Berry's Creek estuarine sediments (Waples et al. 2005; Graham et al. 2012).

As shown in Figure 5, AC added to sediment produced a strong effect. Over the 28-d exposure period, sediment amended with AC contained significantly less MeHg in both the solid phase ($p < 0.001$, $n = 10$) and porewater ($p < 0.001$, $n = 10$) compared with unamended sediment (Supplemental Data, Figure S6 and Tables S12 and S13). The C_{pw} in amended beakers remained <1 ng L^{-1} throughout the study, comparable to background levels in uncontaminated sediments and soils. Sediment–water partitioning, log K_d, was 4.06 without amendment and 4.72 with AC. Sampler–water partitioning in amended sediment was somewhat stronger than in unamended sediment (log $K_{PW} = 4.09$ vs 3.59)

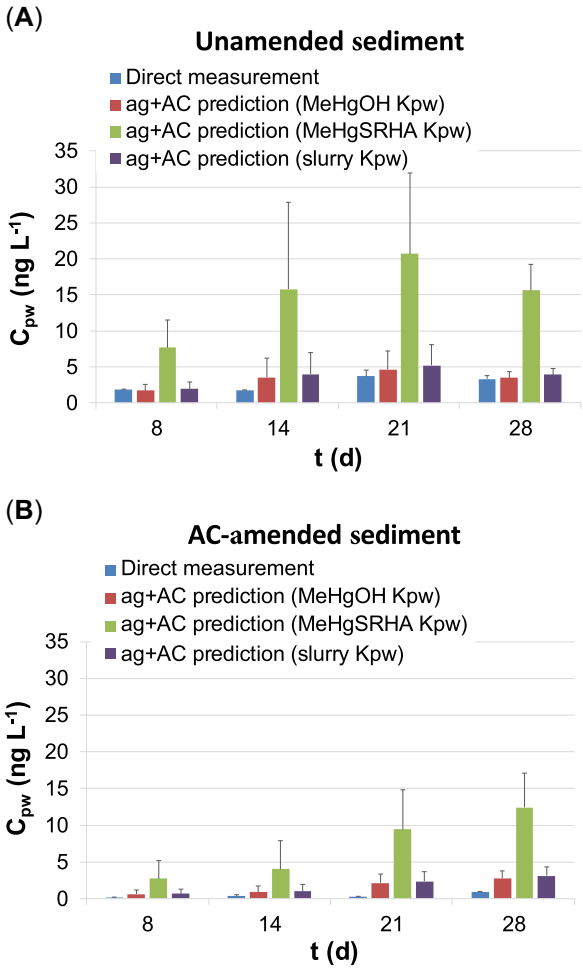

FIGURE 5: Porewater methylmercury (MeHg) concentrations in static sediment microcosm experiment. (**A**) Unamended sediment; (**B**) sediment amended with 5% dry weight activated carbon (AC). Values were directly measured (blue) or predicted by applying ag+AC C_{ps} to linear fits from MeHgOH isotherm (red) or MeHg Suwannee River humic acid (SRHA) isotherm (green) or by dividing C_{ps} by K_{PW} determined from soil slurry experiment (purple). Error bars show +1 standard error ($n = 2$). ag = agarose; K_{PW} = sediment–porewater partition coefficient.

and led to overpredictions of C_{pw}, but even these were within 2 ng L^{-1} of direct measurements.

To explain the apparent effect of AC on K_{PW}, we considered the possibility that AC scavenged DOM, resulting in a smaller fraction of MeHg complexed by DOM and an accordingly higher availability of MeHg to samplers. In fact, at days 14, 21, and 28, DOC concentrations were somewhat lower (not statistically significant) in AC-amended sediment, but our speciation modeling still predicted complete complexation with DOM in all beakers. However, because of the uncertainties inherent in the modeling approach—the most important of which surround the stability constants used for complexation with sulfide and DOM, as well as the fraction of -RSH groups on DOM (see Supplemental Data, Table S4, for details; Liem-Nguyen et al. 2017; Graham et al. 2017)—the hypothesis that AC may alter MeHg speciation by reducing DOC and/or sulfide concentrations should not be discarded at this time. Across all time points and both amendments, sampler

accumulation was reasonably well correlated with directly measured C_{pw} ($r^2 = 0.69$; Supplemental Data, Figure S7).

The microcosm experiment also provided the first temporal results for our samplers in environmentally representative matrices (Figure 5). In both amendment scenarios, there was no trend in the accuracy of sampler-predicted C_{pw} with time. There was a slight increase in C_{pw} with time that was reflected in both direct and sampler measurements. In unamended sediment, the most accurate prediction (using the slurry K_{PW}) was made at 8 d, the first time point sampled (Figure 5A). This gives an indication that ag+AC may achieve equilibrium with porewater in a stagnant deployment on the order of 1 to 2 wk, similar to the measured kinetics in water alone (Figure 2A).

Implications

We report the identification and testing of several sorbent materials with strong potential as passive samplers for $MeHg_{CL}$ in soil and sediment porewaters, including at least one, ag+AC, that functions in a dynamic equilibrium mode. This sampler, along with others designed for chemisorption at reduced-sulfur sites, made reasonably accurate measurements of dissolved MeHg across a range of environmentally realistic matrices including sediments with and without AC amendment. The partitioning coefficients of these samplers are such that a square piece approximately 1 cm on a side will accumulate a readily quantifiable mass of MeHg at a water concentration as low as 1 ng L^{-1}. Importantly, sampler partitioning in slurries and microcosms was generally within approximately half a log unit of the native K_d values in source soils and sediments. Samplers suffered no apparent degradation or fouling during deployment in sediments and soils, indicating that they should not require a potentially interfering membrane (Pham et al. 2015).

Several lines of future investigation are available. Sampler design and fabrication must be optimized and standardized for reproducibility. The potential use of stable MeHg isotopes as performance reference compounds to measure and account for nonequilibrium should be explored. The dynamics of MeHg exchange among samplers, water, and soil/sediment and among different complexing ligands must be elucidated to identify the pools accessed by the samplers and to determine the ability of samplers to respond to fluctuating C_{pw}. This will help to explain observed differences in sampler partitioning across different porewater chemistries and amendment scenarios. Because the utility of the devices will ultimately be determined by their ability to predict benthic bioavailability in diverse field conditions, tests in multiple sediments and alongside organisms in both the laboratory and the field will be necessary. Finally, the sorbents in our samplers have affinity for other metals, including Hg_i, Cd, Pb, and Zn. With additional experimentation, it should be possible to adapt this sampling strategy to measure these metals as well.

Supplemental Data—The Supplemental Data are available on the Wiley Online Library at DOI: 10.1002/etc.4631. The Supplemental Data contain photos, modeling inputs, quality assurance data, detailed analytical procedures, experimental data, and further discussion and figures.

Acknowledgment—The present study was supported by funding from the Strategic Environmental Research and Development Program–Environmental Security Technology Certification Program (ER-2540), the National Institute of Environmental Health Sciences' R01 program (R01ES024284), and The Dow Chemical Company. We thank J.T. Bell, N. Butera, and A. Soren at the Smithsonian Environmental Research Center for laboratory and field assistance. Smithsonian Environmental Research Center Research Experiences for Undergraduates students C. Schuler and M. Sobel contributed to the study. Some Berry's Creek samples were collected by L. Brussel of Parsons. Current address of J.P. Sanders is US Environmental Protection Agency, Washington, DC. Current address of A. McBurney is Alcami, Wilmington, North Carolina, USA. Current address of G.E. Schwartz is Environmental Sciences Division, Oak Ridge National Laboratory, Oak Ridge, Tennessee, USA.

Data Availability Statement—Primary experimental data are provided in the Supplemental Data.

REFERENCES

Aiken GR, Hsu-Kim H, Ryan JN. 2011. Influence of dissolved organic matter on the environmental fate of metals, nanoparticles, and colloids. *Environ Sci Technol* 45:3196–3201.

Amirbahman A, Massey DI, Lotufo G, Steenhaut N, Brown LE, Biedenbach JM, Magar VS. 2013. Assessment of mercury bioavailability to benthic macroinvertebrates using diffusive gradients in thin films (DGT). *Environ Sci Process Impacts* 15:2104–2114.

Balnois E, Wilkinson KJ, Lead JR, Buffle J. 1999. Atomic force microscopy of humic substances: Effects of pH and ionic strength. *Environ Sci Technol* 33:3911–3917.

Benoit JM, Gilmour CC, Mason RP. 2001. The influence of sulfide on solid phase mercury bioavailability for methylation by pure cultures of *Desulfobulbus propionicus* (1pr3). *Environ Sci Technol* 35:127–132.

Bernkop-Schnürch A, Kast CE, Richter MF. 2001. Improvement in the mucoadhesive properties of alginate by the covalent attachment of cysteine. *J Control Release* 71:277–285.

Bhalekar M, Mangesh B, Savita S, Shamkant S. 2013. Synthesis and characterization of a cysteine xyloglucan conjugate as mucoadhesive polymer. *Braz J Pharm Sci* 49:285–292.

Bigham GN, Murray KJ, Masue-Slowey Y, Henry EA. 2016. Biogeochemical controls on methylmercury in soils and sediments: Implications for site management. *Integr Environ Assess Manag* 13:249–263.

Boyd GE, Adamson AW, Myers LS Jr. 1947. The exchange adsorption of ions from aqueous solutions by organic zeolites. II. Kinetics. *J Am Chem Soc* 11:2836–2848.

Burgess RM, Berry WJ, Mount DR, Di Toro DM. 2013. Mechanistic sediment quality guidelines based on contaminant bioavailability: Equilibrium partitioning sediment benchmarks. *Environ Toxicol Chem* 32:102–114.

Chen CY, Borsuk ME, Bugge DM, Hollweg T, Balcom PH, Ward DM, Williams J, Mason RP. 2014. Benthic and pelagic pathways of methylmercury bioaccumulation in estuarine food webs of the northeast United States. *PLoS One* 9:e89305.

Choi J-H. 2010. Fabrication of a carbon electrode using activated carbon powder and application to the capacitive deionization process. *Sep Purif Technol* 70:362–366.

Choi MH, Cech JJJ, Lagunas-Solar MC. 1998. Bioavailability of methylmercury to Sacramento blackfish (*Orthodon microlepidotus*): Dissolved organic carbon effects. *Environ Toxicol Chem* 17:695–701.

Clarisse O, Dimock B, Hintelmann H, Best EP. 2011. Predicting net mercury methylation in sediments using diffusive gradient in thin films measurements. *Environ Sci Technol* 45:1506–1512.

Clarisse O, Foucher D, Hintelmann H. 2009. Methylmercury speciation in the dissolved phase of a stratified lake using the diffusive gradient in thin film technique. *Environ Pollut* 157:987–993.

Clarisse O, Hintelmann H. 2006. Measurements of dissolved methylmercury in natural waters using diffusive gradients in thin film (DGT). *J Environ Monit* 8:1242–1247.

Clarisse O, Lotufo GR, Hintelmann H, Best EP. 2012. Biomonitoring and assessment of monomethylmercury exposure in aqueous systems using the DGT technique. *Sci Total Environ* 416:449–454.

Davison W, Zhang H. 2012. Progress in understanding the use of diffusive gradients in thin films (DGT)—Back to basics. *Environ Chem* 9:1–13.

Dočekalová H, Diviš P. 2005. Application of diffusive gradient in thin films technique (DGT) to measurement of mercury in aquatic systems. *Talanta* 65:1174–1178.

Driscoll CT, Mason RP, Chan HM, Jacob DJ, Pirrone N. 2013. Mercury as a global pollutant: Sources, pathways, and effects. *Environ Sci Technol* 47:4967–4983.

Duan X, Lewis RS. 2002. Improved haemocompatibility of cysteine-modified polymers via endogenous nitric oxide. *Biomaterials* 23:1197–1203.

Fernández-Gómez C, Bayona JM, Díez S. 2014. Comparison of different types of diffusive gradient in thin film samplers for measurement of dissolved methylmercury in freshwaters. *Talanta* 129:486–490.

Fernández-Gómez C, Bayona JM, Díez S. 2015. Diffusive gradients in thin films for predicting methylmercury bioavailability in freshwaters after photodegradation. *Chemosphere* 131:184–191.

Gao Y, De Canck E, Leermakers M, Baeyens W, Van Der Voort P. 2011. Synthesized mercaptopropyl nanoporous resins in DGT probes for determining dissolved mercury concentrations. *Talanta* 87:262–267.

Gao Y, De Craemer S, Baeyens W. 2014. A novel method for the determination of dissolved methylmercury concentrations using diffusive gradients in thin films technique. *Talanta* 120:470–474.

Gilmour CC, Riedel GS, Riedel G, Kwon S, Landis R, Brown SS, Menzie CA, Ghosh U. 2013. Activated carbon mitigates mercury and methylmercury bioavailability in contaminated sediments. *Environ Sci Technol* 47:13001–13010.

Gomez-Eyles JL, Yupanqui C, Beckingham B, Riedel G, Gilmour C, Ghosh U. 2013. Evaluation of biochars and activated carbons for in situ remediation of sediments impacted with organics, mercury, and methylmercury. *Environ Sci Technol* 47:13721–13729.

Graham AM, Aiken GR, Gilmour CC. 2012. Dissolved organic matter enhances microbial mercury methylation under sulfidic conditions. *Environ Sci Technol* 46:2715–2723.

Graham AM, Cameron-Burr KT, Hajic HA, Lee C, Msekela D, Gilmour CC. 2017. Sulfurization of dissolved organic matter increases Hg-sulfide-dissolved organic matter bioavailability to a Hg-methylating bacterium. *Environ Sci Technol* 51:9080–9088.

Haitzer M, Aiken GR, Ryan JN. 2002. Binding of mercury(II) to dissolved organic matter: The role of the mercury-to-DOM concentration ratio. *Environ Sci Technol* 36:3564–3570.

Hong Y, Dan NP, Kim E, Choi H-J, Han S. 2014. Application of diffusive gel-type probes for assessing redox zonation and mercury methylation in the Mekong Delta sediment. *Environ Sci Process Impacts* 16:1799–1808.

Hong YS, Rifkin E, Bouwer EJ. 2011. Combination of diffusive gradient in a thin film probe and IC-ICP-MS for the simultaneous determination of CH_3Hg^+ and Hg^{2+} in oxic water. *Environ Sci Technol* 45: 6429–6436.

Hosse M, Wilkinson KJ. 2001. Determination of electrophoretic mobilities and hydrodynamic radii of three humic substances as a function of pH and ionic strength. *Environ Sci Technol* 35:4301–4306.

Jeremiason JD, Portner JC, Aiken GR, Hiranaka AJ, Dvorak MT, Tran KT, Latch DE. 2015. Photoreduction of Hg(ii) and photodemethylation of methylmercury: The key role of thiol sites on dissolved organic matter. *Environ Sci Process Impacts* 17:1892–1903.

Jiménez Piedrahita ME. 2017. Interpreting DGT measurements beyond steady-state and perfect-sink conditions. PhD thesis, Universitat de Lleida, Lleida, Spain.

Leaner JJ, Mason RP. 2002. Factors controlling the bioavailability of ingested methylmercury to channel catfish and Atlantic sturgeon. *Environ Sci Technol* 36:5124–5129.

Liem-Nguyen V, Skyllberg U, Björn E. 2017. Thermodynamic modeling of the solubility and chemical speciation of mercury and methylmercury driven by organic thiols and micromolar sulfide concentrations in boreal wetland soils. *Environ Sci Technol* 51:3678–3686.

Liu J, Feng X, Qiu G, Anderson CWN, Yao H. 2012. Prediction of methyl mercury uptake by rice plants (*Oryza sativa* L.) using the diffusive gradient in thin films technique. *Environ Sci Technol* 46:11013–11020.

Lu XX, Hong Y, Reible DD. 2014. Assessing bioavailability of hydrophobic organic compounds and metals in sediments using freely available porewater concentrations. In Reible DD, ed, *Processes, Assessment and Remediation of Contaminated Sediments*. Springer, New York, NY, USA, pp 177–196.

Luengen AC, Fisher NS, Bergamaschi BA. 2012. Dissolved organic matter reduces algal accumulation of methylmercury. *Environ Toxicol Chem* 31:1712–1719.

Marvin-DiPasquale M, Lutz MA, Brigham ME, Krabbenhoft DP, Aiken GR, Orem WH, Hall BD. 2009. Mercury cycling in stream ecosystems. 2. Benthic methylmercury production and bed sediment–pore water partitioning. *Environ Sci Technol* 43:2726–2732.

Mason RP. 2001. The bioaccumulation of mercury, methylmercury and other toxic elements into pelagic and benthic organisms. In Newman NC, Roberts MHJ, Hale RC, eds, *Coastal and Estuarine Risk Assessment*. CRC, Boca Raton, FL, USA, pp 127–150.

Merritt KA, Amirbahman A. 2007. Mercury mobilization in estuarine sediment porewaters: A diffusive gel time-series study. *Environ Sci Technol* 41:717–722.

Mohan D, Dines M, Gupta VK, Srivastava SK, Chander S. 2001. Kinetics of mercury adsorption from wastewater using activated carbon derived from fertilizer waste. *Colloids Surf A Physicochem Eng Asp* 177:169–181.

Ndu U, Barkay T, Schartup AT, Mason RP, Reinfelder JR. 2015. The effect of aqueous speciation and cellular ligand binding on the biotransformation and bioavailability of methylmercury in mercury-resistant bacteria. *Biodegradation* 27:29–36.

Ndu U, Christensen GA, Rivera NA, Gionfriddo CM, Deshusses MA, Elias DA, Hsu-Kim H. 2018. Quantification of mercury bioavailability for methylation using diffusive gradient in thin-film samplers. *Environ Sci Technol* 52:8521–8529.

Noh S, Hong YS, Han S. 2016. Application of diffusive gradients in thin films and core centrifugation methods to determine inorganic mercury and monomethylmercury profiles in sediment porewater. *Environ Toxicol Chem* 35:348–356.

Pacific Northwest National Laboratory. 2009. SAMMS® technical summary. Richland, WA, USA. [cited 2018 September 4]. Available from: https://clu-in.org/download/contaminantfocus/sediments/sammstech_summary.pdf

Peijnenburg WJ, Teasdale PR, Reible D, Mondon J, Bennett WW, Campbell PG. 2014. Passive sampling methods for contaminated sediments: State of the science for metals. *Integr Environ Assess Manag* 10:179–196.

Pernodet N, Maaloum M, Tinland B. 1997. Pore size of agarose gels by atomic force microscopy. *Electrophoresis* 18:55–58.

Pham AL-T, Johnson C, Manley D, Hsu-Kim H. 2015. Influence of sulfide nanoparticles on dissolved mercury and zinc quantification by diffusive gradient in thin-film passive samplers. *Environ Sci Technol* 49:12897–12903.

Schwartz GE, Sanders JP, McBurney A, Ghosh U, Gilmour CC. 2019. Impact of dissolved organic matter on mercury and methylmercury sorption to activated carbon in soils: Implications for remediation. *Environ Sci Process Impacts* 21:485–496.

Skyllberg U. 2008. Competition among thiols and inorganic sulfides and polysulfides for Hg and MeHg in wetland soils and sediments under suboxic conditions: Illumination of controversies and implications for MeHg net production. *J Geophys Res* 113:G00C03.

Waples JS, Nagy KL, Aiken GR, Ryan JN. 2005. Dissolution of cinnabar (HgS) in the presence of natural organic matter. *Geochim Cosmochim Acta* 69:1575–1588.

Yu Y, Addai-Mensah J, Losic D. 2012. Functionalized diatom silica microparticles for removal of mercury ions. *Sci Technol Adv Mater* 13:015008.

Zhang JZ, Wang FY, House JD, Page B. 2004. Thiols in wetland interstitial waters and their role in mercury and methylmercury speciation. *Limnol Oceanogr* 49:2276–2286.

